Iranian Journal of
Marine Technology
Marine Science University of Imam Khomeini

PSO-Optimized Blind Image De-convolution for Improved Detectability in Poor Visual Conditions

M. A. Mansoori, M. R. Mosavi, M. H. Bisjerdi

M_Mosavi@iust.ac.ir

The authors are with the Department of Electrical Engineering, Iran University of Science and Technology

Abstract: Image restoration is a critical step in many vision applications. Due to the poor quality of Passive Millimeter Wave (PMMW) images, especially in marine and underwater environment, developing strong algorithms for the restoration of these images is of primary importance. In addition, little information about image degradation process, which is referred to as Point Spread Function (PSF), makes the problem more challenging. Blind image deconvolution is a popular approach for image restoration, which can estimate the original image and the degradation function simultaneously. This is an ill-posed inverse problem and requires regularization to be solved. In addition to the type of regularization functions, the value of regularization parameters can drastically affect the output result. In this paper, we propose an optimized main function for improving the resolution of Passive Millimeter Wave (PMMW) images based on the semi-blind deconvolution and propose a Particle Swarm Optimization (PSO) algorithm for selecting optimum values of regularization parameters in blind image deconvolution. A new cost function is defined for the optimization process which is useful in image restoration. The algorithm has been tested on standard images and evaluated using standard metrics. Two real PMMW images blurred by an unknown degradation function are also used in this algorithm to obtain a sharp deblurred image with an estimate of the PSF. Simulation results show that the proposed method improves the quality of the estimated PSF and the deblurred image.

Key words: Blind deconvolution, PSO algorithm, PSF estimation, PMMW images, Regularization parameter.

Received Date : 1397/06/12
Accepted Date : 1397/11/28

1. Introduction

Passive Millimeter Wave (PMMW) images are obtained through the passive detection of naturally occurring millimeter-wave radiation from a scene. PMMW imaging systems have the ability to form images in low visibility conditions, such as haze, fog, clouds, and even through clothing. These imaging systems provide penetrability through a variety of low-visibility conditions, making them a great candidate for several applications, including maritime surveillance and security, vessel navigation, oil-spill detection, concealed objects detection, and security check at airports, railway, harbors, and etc.

The limitation of PMMW imaging is that image sharpness or resolution is degraded compared to visible and IR images. The other limitation in PMMW images is the effect of noise [1]. For improving the quality of degraded PMMW images, image restoration or deblurring methods can be used. When there is not enough information about the degradation process, blind image deconvolution is a more effective method.

Blind image restoration is the process of estimating both the true image and the blur from the degraded image characteristics, using partial information about the imaging system. The goal of blur identification is to estimate the attributes of the imperfect imaging system from the observed degraded image. The combination of image restoration and blur identification is often referred to as blind image deconvolution [2]. In most cases, the causes of image degradation can be categorized as motion blur, out of focus blur, and atmospheric turbulence blur. Mathematically, blurring degradation can be modeled as the following equation:

$$g(x,y) = h(x,y) * f(x,y) + n(x,y) \tag{1}$$

where g(x,y) is the degraded image, h(x,y) is the Point Spread Function (PSF), f(x,y) is the original image, (*) denotes the convolution operator, and n(x,y) is the additive noise which is often considered to be white Gaussian noise.

When h(x,y) is equal to the identity operator, the problem reduces to the image denoising. There exists a wide range of techniques for different applications. For example, [3] proposes a filter which uses circular mean points to reduce noise effects, and in research by [4], a two-dimensional adaptive filter is introduced for image denoising.

In classical non-blind image restoration methods, PSF is assumed to be known, and the aim is to find an estimate of f(x,y), given both h(x,y) and the degraded image. Inverse filtering, Lucy Richardson algorithm, Wiener filtering, and deconvolution using regularized filter are some conventional methods for non-blind image restoration [5,6]. Although in non-blind image deconvolution PSF is known, the problem is still challenging, and several techniques are proposed in these years to improve the quality of the restored image [7-9].

Blind image deconvolution is a more sophisticated problem, whose objective is to estimate the original image and the true PSF. The only available information is the observed image and prior information about the PSF or the original image. This is an ill-posed inverse problem and one requires regularization technique for solving this kind of problems. Maximum a posteriori solution, variational Bayesian approach, auto-recursive moving average parameter estimation, and non-parametric deterministic constraints algorithms are some methods for solving blind deconvolution problems. Interested readers may refer to [2] and [10] to review blind deconvolution algorithms. Regularization-based blind image restoration can be considered as a special case of Bayesian inference methods in the general Bayesian framework.

The problem of blind image deconvolution can be formulated by the following joint minimization problem using regularization of both the original image and the PSF:

$$\min_{f,h} \| f * h - g \|_2^2 + \lambda_1 R_1(f) + \lambda_2 R_2(h) \tag{2}$$

where the first term is called data fidelity, R1 and R2 are regularization functions, and λ1 and λ2 are regularization parameters. Selecting appropriate regularization function and parameter for both the image and the blur kernel is of primary importance. Based on the application, one should choose the best function and parameter. For example, Almeida proposed a new edge detector for regularization function, which assumes that the edges of a natural image are sparser than a blurred one [11]. Liao used Total Variation (TV) regularization for both the image and the kernel [12]. He also proposed a Generalized Cross Validation (GCV) approach for automatically selecting the regularization parameters. In [13], framelet regularization is employed for Passive Millimeter Wave (PMMW) images. In addition, the kernel prior is L2-norm of the gradient. Raun et al. introduced a new spatially weighted total variation regularization model for the PMMW image prior, and the kernel is assumed to be Gaussian [14]. In [15] a combination of Huber functions is used for the image regularizer. The function inputs are finite-difference approximations of second order derivatives. Krishnan et al. introduced a new sparsity measure based on L1/L2 norm ratio. It is demonstrated that the new measure is a better regularization term than conventional sparsity measures [16]. H. Ji et al. employed the ratio of L1 to L2 norm for wavelet coefficients, as a new regularizer for the original image [17]. In [18], Tikhonov regularization is used, and for the determination of the regularization parameter, a GCV algorithm is used. The GCV function is minimized using a Particle Swarm Optimization (PSO) algorithm. However, the method is non-blind and there is only one variable to be tuned. In addition, the Tikhonov function can lead to over-smoothing.

Regularization parameters play an important role in image deconvolution. If the parameters are too large, the restored image does not fit to the given data, and if they are too small, the solution is under-smooth, and the noise is not eliminated properly. Ideally, an optimum parameter is obtained when the Mean Square Error (MSE) between the original image and the restored image is minimized. However, the computation of MSE is impossible because the original image is not available [19].

All of the above-mentioned methods are sensitive to the regularization parameters, and the best values of these parameters must be manually selected to obtain better results. In this paper, we propose a new method based on PSO algorithm for selecting optimum values of regularization parameters automatically, which we call PSO-optimized blind image deconvolution. The improved method is robust to noise and blur and therefore is very effective in PMMW images.

It should be noted that the PMMW images used in this paper are for the concealed object detection application. However, the proposed algorithm can be used for other PMMW imaging applications, including underwater and marine security.

The rest of the paper is as follows. In section 2, the blind deconvolution algorithm is explained, and the details of regularization functions are described. In section 3, our proposed method is explained and the objective function in our PSO algorithm is described. In section 4 experimental results are presented. Section 5 presents the conclusion.

2. Blind Deconvolution Method

The blind deconvolution method used in this paper is based on reference [16], in which Krishnan demonstrated that the normalization of L1-norm results in a better choice for the regularization function in blind image deconvolution.

2.1. Regularization Function

Regularization functions based on L1-norm and L2-norm of the image (or the derivative of the image) have a major drawback; the amount of these norms decreases by increasing the amount of blur. As a result, by minimizing these norms, one cannot eliminate the blur from the degraded image. L1/L2 norm, however, has overcome this drawback due to the increasing characteristics of the cost function with respect to the blur amount.

In [20] it is shown that the normalization of L1-norm does not work well for all types of images. However, we observed that the new regularization function is applicable to our sample images. The first image is the cameraman, and the second one is the image of concentric circles. These images are blurred by a Gaussian PSF with a variable size, and then the values of corresponding norms are measured. In Fig. 1, the behavior of the conventional regularization functions is compared with the ratio of L1 to L2 norm for these images.

For both images, the cost function for L1-norm and L2-norm decreases by increasing the blur amount, while the ratio between them is an increasing function. The reason why we used this regularization function for our sample images was the increasing behavior of normalized L1-norm for concentric circles.

2.2. Solving Joint Minimization Problem

Obtaining the desired sharp image and the true PSF is dependent on how the joint minimization problem is solved. By considering the abovementioned image regularization term, and the L1-norm for the kernel, the joint minimization problem in the derivative domain can be written as [16]:

$$\min_{x,k} \lambda\|x * k - y\|_2^2 + \frac{\|x\|_1}{\|x\|_2} + \psi\|k\|_1 \tag{3}$$

where y is the blurred image in high frequencies, x is the unknown sharp image in high frequencies, and λ and ψ are the regularization parameters. Note that by dividing the above equation by λ, the equation can be rewritten as Eq. (2), therefore λ and ψ play the same role as $\lambda 1$ and $\lambda 2$. Minimization of Eq. (3) gives the restored image and the estimated kernel. The first term in Eq. (3) takes into account the formation model in Eq. (1). The second term is the new regularizer which encourages sparsity in the reconstruction. To reduce noise in the kernel, the L1 regularization is added on k in the third term.

In order to solve Eq. (3), an alternative minimization algorithm must be used because the problem is strictly non-convex. After x and k initialization, the first step is to fix k and minimize the following problem, which is called x-update step [16]:

$$\min_{x} \lambda\|x * k - y\|_2^2 + \frac{\|x\|_1}{\|x\|_2} \tag{4}$$

The second step is to fix the updated x, and minimize the following problem, which is called k-update step [16]:

$$\min_{k} \lambda\|x * k - y\|_2^2 + \psi\|k\|_1 \tag{5}$$

For the x-update and k-update step, respectively, iterative shrinkage algorithm in association with fixed-point iteration and an iterative reweighted Least Square algorithm is used to minimize the corresponding cost functions. Finally, after estimating the PSF from the previous, a non-blind image deconvolution algorithm is used to recover the original image step [16].

3. Proposed Method

3.1. Proposed Main Function

The formulation of proposed main function is presented in the following. $\phi_{p_{adapt}}$ is a Gaussian filter with an adaptive standard deviation.

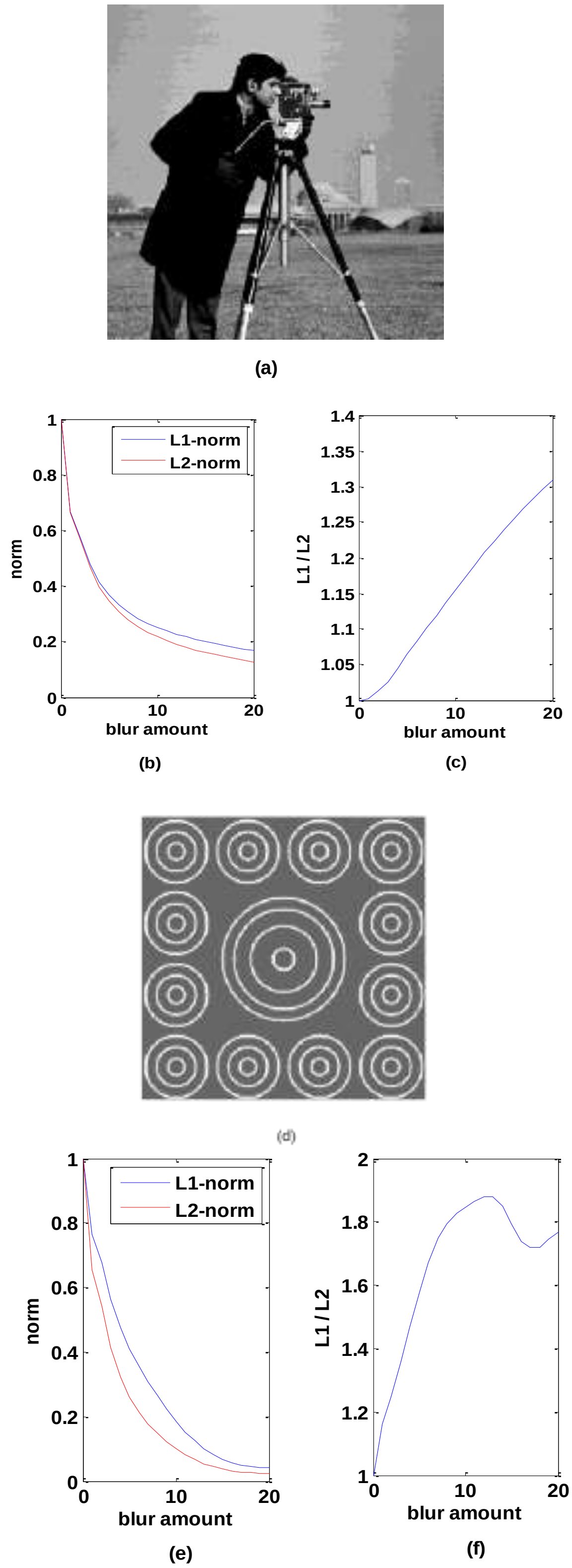

Fig.1 Standard comparison of the conventional regularization functions with L1 to L2 norm: (a) original cameraman image, (b) conventional norm values for cameraman image, (c) L1/L2 norm values for cameraman image, (d) original concentric circles image, (e) conventional norm values for concentric circles image, and (f) L1/L2 norm values for concentric circles image.

This filter is convolved with the image obtained from $(y-\phi_h * f_{est})$ part. $\phi_{p_{adapt}}$ is presented in Eq. (6):

$$\phi_{p_{adapt}} = \frac{1}{2\pi p_{adapt}^{\ 2}} \exp\left(-\frac{x^2+y^2}{2p_{adapt}^{\ 2}}\right)$$

$$p_{adapt} = \begin{cases} \xi & j > \min(\mathrm{J}) \quad and \quad j < \min(\mathrm{J}) + \Lambda \\ \xi - 0.2 & j \geq \min(\mathrm{J}) + \Lambda \quad and \quad j < \min(\mathrm{J}) + 2\times\Lambda \\ \xi - 0.4 & j \geq \min(\mathrm{J}) + 2\times\Lambda \quad and \quad j \leq \max(\mathrm{J}) \end{cases} \tag{6}$$

$$\Lambda = \left(\frac{\max(\mathrm{J}) - \min(\mathrm{J})}{n}\right)$$

In the above equation, p_{adapt} depends on entropy of any point of the image. In Eq. (6), j is entropy of the intent pixel. J is the matrix that contains entropy of all pixels and Λ is a range of entropies. Also, ξ is considered 2.1 for all noises and obtained experimentally. In this paper, n is considered as three, and shows the number of the entropy epoch. If entropy of the image is relatively higher, p_{adapt} would be smaller to smooth the content less (correspondent to third term) and if entropy is relatively lower, p_{adapt} would be higher which will eliminate noise well. Wavelet-based noise reduction part of cost function, add extra content that is called ringing effect. Ringing effect has structure despite of noise and proposed adaptive filter cannot eliminate it.

Since the ringing has intense destructive effect in higher iteration, a new operator is added to eliminate this structure. Also, in order to resolve problems caused by noise removal function, R_1, which cannot be solved using p_{adapt}, non-linear function F is defined. In this sense, this function is multiplied by the image resulting from $\phi_p * (y-\phi_h * f_{est})$ and its values at any point are obtained from Eq. (7). This function removes problems caused by noise removal function and p_{adapt} cannot solve them properly.

$$F = e^{-\left(\frac{1}{J_{i,j} - \min(\mathrm{J})}\right)} \tag{7}$$

Where $J_{i,j}$ expresses entropy for each pixel, $\min(\mathrm{J})$ expresses the lowest entropy in the whole image, val is the amount of each pixel in the mask. Fig.2a shows degraded image. As it can be seen in section (b) of Fig.2, small circular scattered points in the whole image are formed by wavelet de-noising operations. In fact, using this method, contents of the image have changed and blobs are added to the image. The second part of the proposed method in Eq. (6) tries to solve this problem and improves the image using iteration.

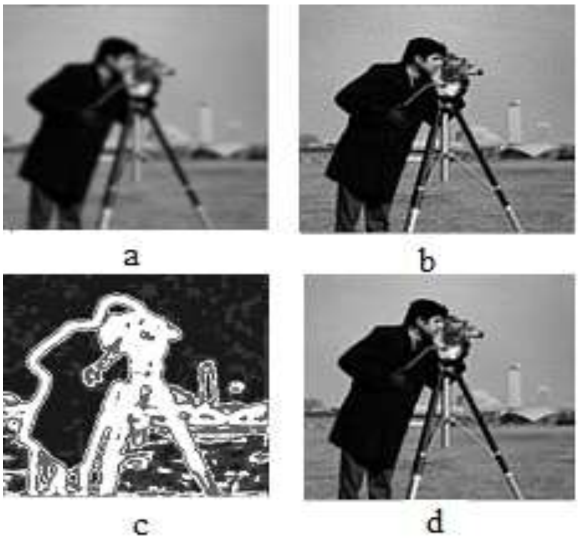

Fig.2 (a) Degraded image, (b) estimated image with ISTA method, (c) designed mask, and (d) estimated image with ISTA method using adaptive filters and mask.

The ringing effect clearly shown in Fig.2. To solve this problem, a mask is designed to eliminate the effects of blobs in the estimated image of the difference image. The purpose of designing this mask is to reset regions with low entropy in the difference image to zero. This mask is designed such that the lower is the entropy of the destructed image, its value would be closer to zero, and the higher is the entropy, its value would be close to one. Fig.2c illustrates the designed mask. Initializing each region of the mask is specified using Eq. (7). Although these blobs are created in the whole image, they are weakened in low entropy regions using a weakening coefficient and get them close to zero. These blobs exist in high entropy regions also, but weakening coefficient cannot be used in these regions, because it destructs the difference image for reducing blurredness.

As shown in section (d) of Fig.2, the blobs that were produced by wavelet de-noising method are eliminated by designed mask. The block diagram of the proposed method is presented in Fig.3.

For the minimization of Eq. (6), an Iterative Shrinkage Thresholding Algorithm (ISTA) is used. Algorithm 1 and Eq. (8), explains the ISTA method for the estimation of the desired image.

The shrinkage operator (S) is defined as:

$$S_T(u) = \max(0, 1 - \frac{T}{|u|})u \qquad (8)$$

Algorithm 1

$$f_{est}^{\ell+1} = f_{est}^{\ell} + F(\phi_{P_{adapt}} * (y - \phi_h * f_{est}))$$
$$f_{est}^{\ell+1} = S_{\tau.\lambda_1}(f_{est}^{\ell+1})$$

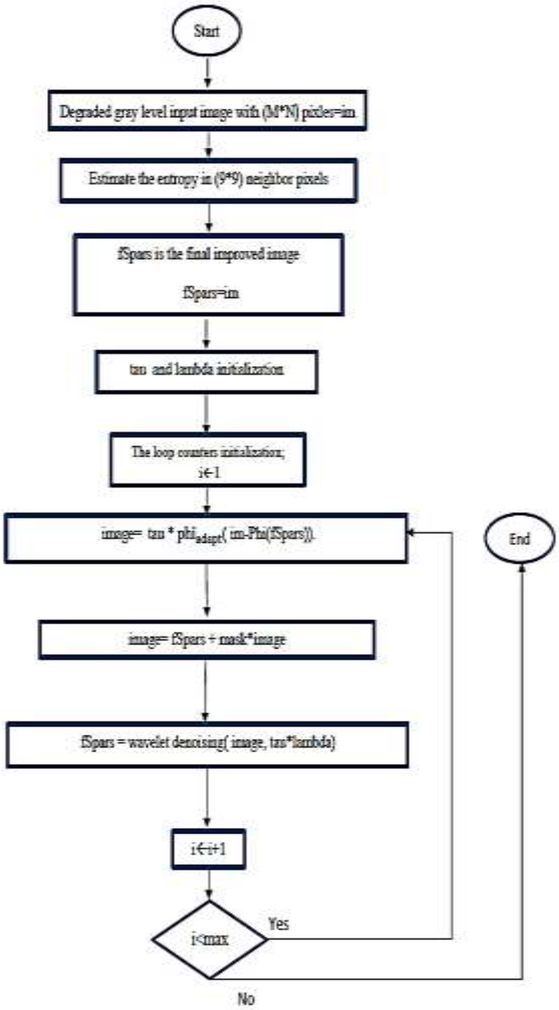

Fig.3 Block diagram of the proposed method.

This operator is applied to the wavelet frame coefficients of the image, and then the image is obtained by using an inverse transform. Initialize τ, λ_1

3.2. Optimization Process

We propose a PSO algorithm for selecting optimum values of regularization parameters. The block diagram of our method is presented in Fig. 4. Desired values of the parameters should result in better estimation of x and k. Parameters that must be optimized are λ and ψ, which form the particles of our PSO algorithm.

Each λ and ψ value will result in a different updated x and k, so the values, which minimize the following cost function, can be considered as the optimum values of the parameters:

$$\min_{\lambda,\psi} \; w\|x_\lambda * k_{\lambda,\psi} - y\|_2^2 + \frac{\|x_\lambda\|_1}{\|x_\lambda\|_2} \qquad (9)$$

where w is a constant weight that is selected according to the size of the PSF. $x\lambda$ and $k\lambda,\psi$ is computed from x-update and k-update using one iteration.

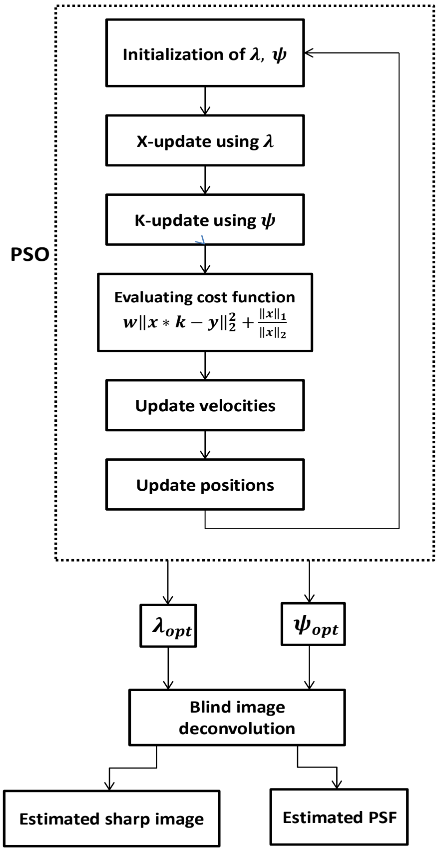

Fig.4 Block diagram of the proposed method based on PSO algorithm.

They are highly dependent on the regularization parameters and their indexes represent this dependency. If the parameters result in a weak estimation of x and k, they will be rejected, due to the high value of the cost function in Eq. (9). On the contrary, a good estimation of x and k means a low value of the cost function, hence obtaining better choices for regularization parameters.

Each particle consists of two parameters: λ and ψ. By Eq.s (4) and (5), we can obtain new x and k. After evaluating the cost function, the velocities and the positions of the particles must be updated. This process will be iterated until the particles converge to the best one. This particle corresponds to the optimal estimation of the PSF and the sharp image in high frequencies. As a result, when we use the obtained λ and ψ as the initialization of the blind image deconvolution, the estimated kernel will be closer to the real PSF. The deblurred image will also be more similar to the original image.

3.3. PSO Algorithm

PSO is a biologically inspired optimization method developed by Eberhart and Kennedy in 1995 based on the social behaviors of birds [21]. Several modifications of PSO are then developed to accelerate achieving the best conditions [22-24]. PSO consists of a swarm of particles where each particle represents a potential solution. The particles fly in a search space based on their own experience (personal best) and also the experience collected from the neighboring particles (global best) in order to find the best position. The position of the particles is influenced by velocity. The position and the velocity of each particle are updated using the following two equations:

$$x_i(t+1)=x_i(t)+v_i(t+1) \tag{10}$$

$$v_i(t)=l\times v_i(t-1)+c_1r_1\left(Pbest(t)-x_i(t-1)\right)$$
$$+c_2r_2\left(Gbest(t)-x_i(t-1)\right) \tag{11}$$

where x is position and v is the velocity of the particles. c1 and c2 are correction factors, r1 and r2 are random numbers, and l is the inertia weight. Pbest and Gbest are computed using an objective function. In the current paper, we define the closeness of the estimated sharp image in high frequencies (x) to the original one, as the objective function.

To measure this closeness, we used the following norms:

$$w\|x*k-y\|_2^2+\frac{\|x\|_1}{\|x\|_2} \tag{12}$$

In the first term, we reblur the estimated sharp image by the estimated kernel, and measure the difference between the reblurred image and the blurred one. In the second term, we compute the ratio of L1-norm to L2-norm of the estimated sharp image. It has a lower value when the blur and noise are significantly removed from the degraded image. Here, the estimated sharp image and the estimated kernel are the updated x and k, by one step, respectively. Consequently, when the updated x and k are closer to the original ones, the total amount of our objective function has its minimum value.

4. Experimental Results

Experiments are done in MATLAB environment to show the performance of the proposed method. We used the image of the cameraman and concentric circles as the standard images. The method has also been tested on two real PMMW images. The standard images are first blurred by a fixed PSF, and then Gaussian noise is added to them. The degraded images are then deblurred by the improved blind deconvolution method, and the results are compared with the original method in [16]. The estimated kernel in each method is also compared with the original PSF. Fig.s 5 and 6 show the final results for the image of the cameraman and concentric circles, respectively.

Peak Signal to Noise Ratio (PSNR) and Structural Similarity Image Index (SSIM) between the restored image and the original image are shown in Table 2. PSNR between the degraded image and the original image is also shown in Table 2 to compare the improvement of PSNR in each method.

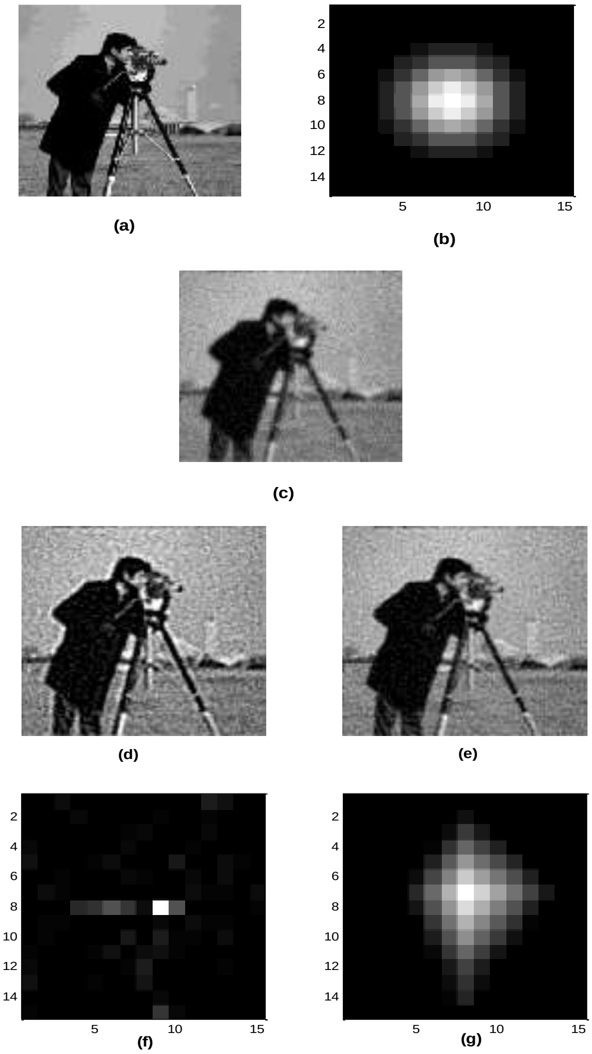

Fig.5 Restored results for the cameraman image: (a) original image, (b) original gaussian PSF of “size = 15” and “standard deviation = 2.1”, (c) blurred and noisy image (zero mean and “variance = 0.003”), (d) restored image for the conventional method, (e) restored image for our proposed method, (f) estimated PSF for the conventional method, and (g) estimated PSF for our proposed method.

As seen in Table 1, Universal Image Quality Index (UIQI) decreases by increasing the amount of noise, but the improved method remarkably enhances the value of UIQI. In the worst case, when the amount of blur and noise have their maximum values (15×15 blur size and 0.005 noise level), the improvement of UIQI is significant. PSNR and SSIM are also enhanced in the proposed method.

To evaluate the performance of the proposed method, we used PSNR and SSIM as the standard metrics for the deblurred images, and the UIQI proposed by Z.

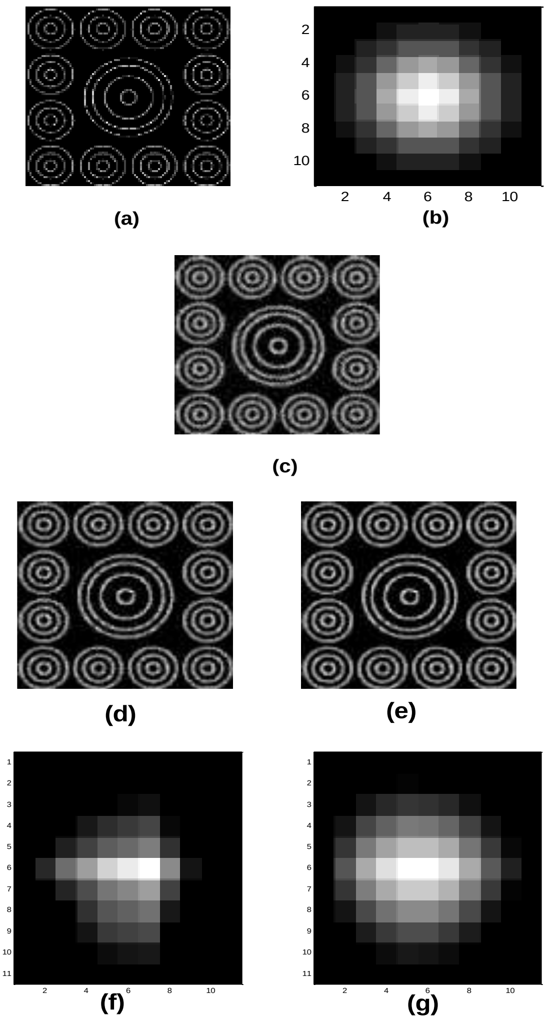

Fig. 6 Restored results for concentric circles image: (a) original image, (b) original gaussian PSF of “size = 11” and “standard deviation = 2.1”, (c) blurred and noisy image (zero mean and “variance = 0.001”), (d) restored image for the conventional method, (e) restored image for our proposed method, (f) estimated PSF for the conventional method, and (g) estimated PSF for our proposed method.

Wang et al. for the estimated kernels. PSNR evaluates the amount of noise in the restored image; SSIM measures the similarity between the restored image and the original one, and UIQI compares the similarity of the estimated kernels.

The images are blurred by a Gaussian PSF of size 11×11 and 15×15, and then Gaussian noise with zero mean and three different variances is added to them. UIQI between the estimated kernel and the true PSF is shown in Table 1.

In order to make fair comparisons between the method in [16] and our proposed method, we fixed the regularization parameters in the method by Krishnan [16] for both images. The values of PSO parameters are selected according to Table 3, but the number of iterations and the value of w in the objective function are slightly different in each experiment in order to get better results.

Table 1 UIQI between estimated and original PSF.

	PSF Size	Noise	UIQI [16]	UIQI [Proposed]
Cameraman	11×11	0.001	0.792	0.887
		0.003	0.141	0.810
		0.005	0.132	0.723
	15×15	0.001	0.907	0.949
		0.003	0.300	0.922
		0.005	0.118	0.780
Circles	11×11	0.001	0. 710	0.899
		0.003	0.155	0.818
		0.005	0.102	0.756
	15×15	0.001	0.690	0.915
		0.003	0.193	0.819
		0.005	0.156	0.724

For PMMW images, the same method is used to estimate the kernel and the original image. One of the important characteristics of PMMW images is the high amount of noise. According to Table 1 and Table 2, the improved method is robust to noise, and therefore compatible with PMMW images. Fig.s 7 and 8 show the final result for two PMMW images. The PSF for most PMMW images are Gaussian type [13,15, 25, 26]. As it can be seen from Fig. 7 and Fig. 8, the estimated kernel in the improved method is more similar to Gaussian function. The estimated image in our method is also sharper than non-improved one. For convenience of comparison, partial close-ups of the same region of the recovered images are shown in Fig. 9 for the first PMMW image. As it can be seen from Fig. 9, the concealed object can be easily identified by the improved method, due to more sharpness of the image.

5. Conclusion

In this paper, we have proposed a semi-blind image deconvolution algorithm based on a new relationship composed of one main and two regularization functions, is defined to get better quality images at the output, and alternative optimization is used to solve proposed relationship.

Furthermore, improvement of the output image was studied with standard measures like PSNR and non-reference for PMMW images. Standard images like cameraman were improved specifically for low noise and significant improvement was observed in visual quality of output images. Also, the proposed method has been tested on two real PMMW images.

To evaluate the performance of the proposed method, we compared the restored image from different methods by a non-reference measure for PMMW images. In comparison with the conventional methods, the proposed approach resulted in higher values of PSNR and other criteria. The estimated PSF from the proposed algorithm was also closer to the original PSF, according to the comparison of the estimated sigma from different methods.

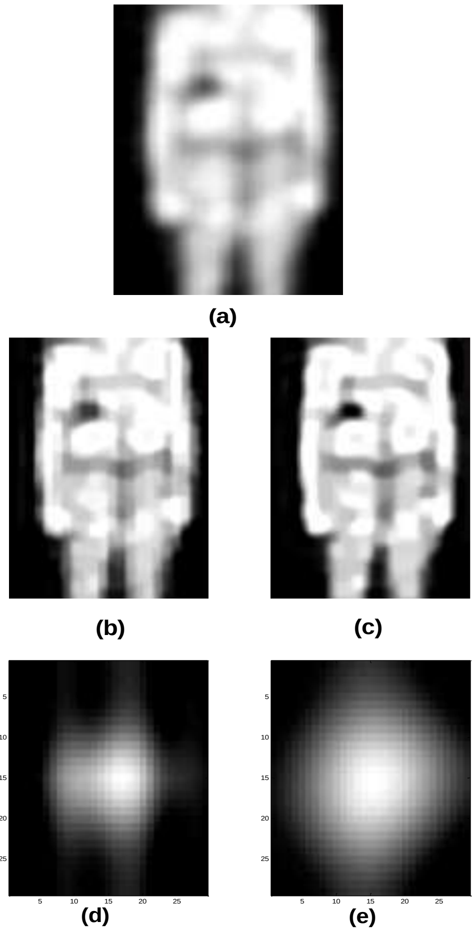

Fig. 7 Restored results for the first PMMW image: (a) observed image, (b) restored image by the conventional method, (c) restored image by the proposed method, (d) estimated PSF by the conventional method, and (e) estimated PSF by the proposed method.

Applying the proposed method on PMMW images with low inherent resolution reduce noise content, improves edges and creates roughness in corners of the image. It is clear that in hidden objects detection application, improving resolution of the images is done with the purpose of better detection of background and the proposed method was confirmed to be effective in this context. Also, in this paper, we have proposed a new method based on PSO algorithm in order to choose better regularization parameters. The method has been tested on two standard images with different blur kernels and noise levels.

To evaluate the estimated kernel and image, three different metrics were used for these images. In comparison with the conventional method, our proposed method resulted in higher values of UIQI, PSNR, and SSIM. Therefore, the estimated kernel and image were more similar to the original ones. Two PMMW images were also used for evaluating the performance of our method.

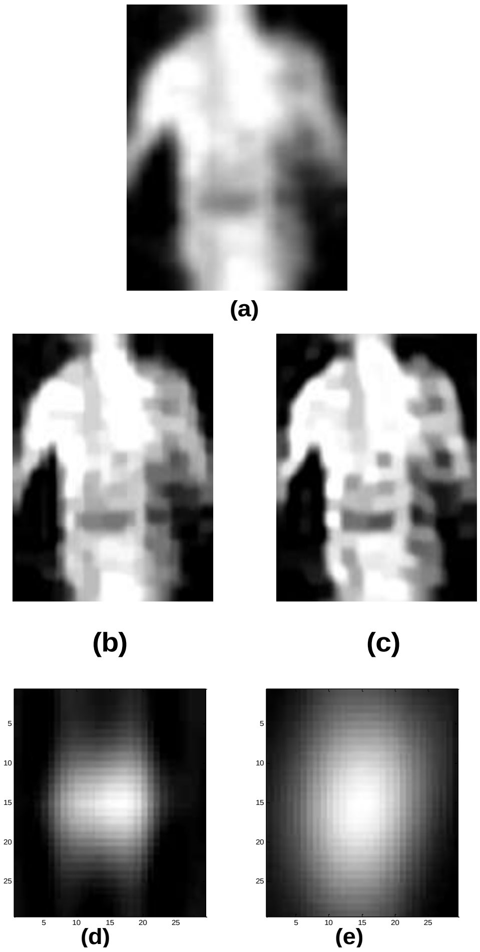

Fig. 8 Restored results for the second PMMW image: (a) observed image, (b) restored image by the conventional method, (c) restored image by the proposed method, (d) estimated PSF by the conventional method, and (e) estimated PSF by the proposed method.

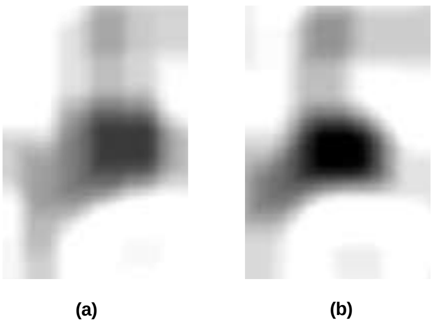

Fig. 9 Concealed object in the first PMMW image, which is obtained by zooming the image: (a) conventional method, and (b) proposed method.

For these images, the original image or the PSF was not available, so we could not compare the methods using the same metrics. However, one can visually observe that the estimated kernel in both images is more similar to a Gaussian function, and the estimated image is also sharper than the conventional method.

Table 2 PSNR and SSIM between the original image and restored image.

	PSF Size	Noise ($\times 10^{-3}$)	PSNR Degraded	PSNR [16]	PSNR [Proposed]	SSIM [16]	SSIM [Proposed]
Cameraman	11×11	1	21.64	22.85	23.02	0.600	0.637
		3	20.56	19.92	21.24	0.282	0.370
		5	19.73	18.12	19.69	0.209	0.260
	15×15	1	21.61	22.96	22.91	0.624	0.652
		3	20.55	19.71	21.40	0.305	0.399
		5	19.71	17.86	19.92	0.207	0.279
Circles	11×11	1	16.23	16.86	16.95	0.346	0.366
		3	15.94	16.46	16.73	0.271	0.231
		5	15.70	15.73	16.51	0.217	0.274
	15×15	1	16.20	16.61	16.94	0.349	0.387
		3	15.92	16.31	16.59	0.280	0.325
		5	15.66	15.76	16.22	0.238	0.307

Table 3 The values of PSO parameters

ℓ	$c_1 = c_2$	Iterations	w
1	2	20	0.4*

* For cameraman image and PSF size equal to 15

Reference

[1] Yujiri, L., Shoucri, M., and Moffa, P., “Passive Millimeter-Wave Imaging”, IEEE Microw. Mag., Vol.4, No.3, pp.39-50, 2003.

[2] Kundur, D. and Hatzinakos, D., “Blind Image Deconvolution”, IEEE Signal Processing Mag., Vol.13, No.3, pp.43-64, 1996.

[3] Shakoor, M.H. and Tajeripour, F., “Circular Mean Filtering for Textures Noise Reduction”, Iranian Journal of Electrical & Electronic Engineering, Vol.11, No.3, pp.1-9, 2015.

[4] Shams, M., Abadi E. and Nikbakht, S., “Image Denoising with Two-Dimensional Adaptive

Filter”, Iranian Journal of Electrical & Electronic Engineering, Vol.7, No.2, pp.84-105, 2011.

[5] Kaur, A. and Chopra, V., “A Comparative Study and Analysis of Image Restoration Techniques using Different Image Formats”, International Journal for Science and Emerging Technologies with Latest Trends, Vol.2, No.1, pp.7-14, 2012.

[6] Umale, S.H. and Sahu, A.M., “A Review on Various Techniques for Image Deploring”, International Journal of Computer Science and Mobile Computing, Vol.3, No.4, pp.263-268, 2014.

[7] Sun, L., Cho, S., Wang, J., and Hays, J., “Good Image Priors for Non-blind De-convolution”, Computer Vision – ECCV 2014 European Conference, Switzerland: Springer International Publishing, 2014.

[8] He, N., Zhang, Q., Chi, Y., and Lu, K., “Image De-convolution using l1 Sparse Regularization”, International Conference on Internet Multimedia Computing and Service, 2015.

[9] Zhang, X., Sun, F., Liu, G., and Ma, Y., “Non-Blind Deblurring of Structured Images with Geometric Deformation”, The Visual Computer, Vol.31, No.2, pp.131-140, 2015.

[10] Campisi, P. and Egiazarian, K., Blind Image Deconvolution: Theory and Applications, Boca Raton, FL: CRC, 2007.

[11] Almeida, M.S.C. and Almeida, L.B., “Blind and Semi-Blind Deblurring of Natural Images”, IEEE Transactions on Image Processing, Vol.19, No.1, pp.36-52, 2010.

[12] Liao, H. and Ng M.K., “Blind Deconvolution using Generalized Cross-Validation Approach to Regularization Parameter Estimation”, IEEE Transactions on Image Processing, Vol.20, No.3, pp.670-680, 2011.

[13] Fang, H. and Yan, L., “Parametric Blind De-convolution for Passive Millimeter Wave Images with Framelet Regularization”, International Journal for Light and Electron Optics, vol.125, No.3, pp.1454-1460, 2014.

[14] Ruan, Y., Fang, H., and Chen, Q., “Semiblind Image Deconvolution with Spatially Adaptive Total Variation Regularization”, Mathematical Problems in Engineering, Vol.2014, pp.1-8, 2014.

[15] Yan, L., Liu, H., Chen, L., Fang, H., Chang, Y., and Zhang, T., “Parametric Semi-Blind De-convolution Algorithm with Huber-markov Regularization for Passive Millimeter-Wave Images”, Journal of Modern Optics, Vol.60, No.12, pp.970-982, 2013.

[16] Krishnan, D., Tay, T., and Fergus, R., “Blind Deconvolution using a Normalized Sparsity Measure”, IEEE Conference on Computer Vision and Pattern Recognition, pp.233-240, 2011.

[17] Ji, H., Li, J., Shen, Z., and Wang, K., “Image Deconvolution using a Characterization of Sharp Images in Wavelet Domain”, Applied and Computational Harmonic Analysis, Vol.32, No.2, pp.295-304, 2012.

[18] Dash, R. and Majhi, B., “Particle Swarm Optimization based Regularization for Image Restoration”, IEEE Conference on Nature & Biologically Inspired Computing, pp.1253-1257, 2009.

[19] Chen, Z., Wang, M., Wen, Y., and Zhu, Z., “Choice of Regularization Parameter in Constrained Total Variational Image Restoration Model”, IEEE International Conference on Computational Intelligence and Security, pp.736-740, 2014.

[20] Chaudhuri, S., Rameshan, R., and Velmurugan, R., “Sparsity-based Blind De-convolution”, Blind Image Deconvolution Methods and Convergence, Switzerland: Springer International Publishing, 2014.

[21] Rini, D.P., Shamsuddin, S.M., and Yuhaniz, S.S., “Particle Swarm Optimization: Technique, System and Challenges”, International Journal of Computer Applications, Vol.14, No.1, pp.19-27, 2011.

[22] Mirjalili, S., Lewis, A., and Sadiq A.S., “Autonomous Particles Groups for Particle Swarm Optimization”, Arabian Journal for Science and Engineering, Vol.39, No.6, pp.4683-4697, 2014.

[23] Hu, W. and Yen, G., “Adaptive Multi-Objective Particle Swarm Optimization based on Parallel Cell Coordinate System”, IEEE Transactions on Evolutionary Computation, Vol.19, No.1, pp.1-18, 2015.

[24] Tang, R. and Fang, Y., “Modification of Particle Swarm Optimization with Human Simulated Property”, Neurocomputing, Vol.153, pp.319-331, 2015.

[25] Luxin, Y., Tianxu, Z., Sheng, Z., Jian, H., and Jianmao, Z., “Study on Multichannel Passive Millimeter-Wave Radiometer Imaging and Superresolution”, International Journal of Infrared and Millimeter Waves, Vol.1006, No.27, pp.1403-1414, 2006.

Mansoori M.A., Mosavi M.R., and Bisjerdi, M.H., “Regularization-Based Semi-Blind Image Deconvolution using an Improved Function for PMMW Images Application”, Journal of Circuits, Systems, and Computers, Vol.27, No.7, pp.1071-1075, 2018.

Authors:

Mohammad-Reza Mosavi (Corresponding Author) received his B.S., M.S., and Ph.D. degrees in Electronic Engineering from Iran University of Science and Technology (IUST), Tehran, Iran in 1997, 1998, and 2004, respectively. He is currently faculty member of

Department of Electrical Engineering of IUST as professor. He is the author of more than 350 scientific publications on journals and international conferences. His research interests include circuits and systems design.

Mohammad-Amir Mansoori received his B.S. degree in Electronic Engineering from Khajeh Nasir Toosi University of Technology (KNTU), Tehran, Iran in 2013, and his M.S. degree in Electronic Engineering from Iran University of Science and Technology (IUST), Tehran, Iran in 2016. His research interests include image processing, hardware design, FPGAs, and embedded vision.

Mohammad-Hossein Bisjerdi received his B.S. and M.S. degrees in Electronic Engineering from shahed University, Tehran, Iran in 2006 and 2009, respectively. He is currently PhD candidate in Electronic Engineering of Department of Electrical Engineering of Iran University of Science and Technology (IUST). His research interests include image processing and circuits and systems design.